Proceedings World Geothermal Congress 2020+1
Reykjavik, Iceland, April - October 2021

The Shape of the Network of Flow Pathways Leading to a Geothermal Well: Informing the Conceptual Model using Fractional Dimension and Boundaries with Numerical Pressure Transient Analysis

Katie McLean [1,2]*, Sadiq J. Zarrouk[1] and Egill Júlíusson[3]

[1] Department of Engineering Science, University of Auckland, Private Bag 90210, Auckland, New Zealand

[2] Contact Energy Ltd., Wairakei Power Station, Taupo, New Zealand

[3] Landsvirkjun, Háaleitisbraut 68, 103 Reykjavík, Iceland

*pmcl037@aucklanduni.ac.nz

Keywords: geothermal, well, shape, flow pathways, conceptual model, numerical, pressure transient analysis, fractional dimension, boundaries.

ABSTRACT

Pressure transient analysis (PTA) has come only relatively recently to the geothermal industry, where it is often performed using simpler analytical tools, which have been shown to be inapplicable to geothermal reservoirs, introducing significant error into the results. The results of PTA have many potential uses, informing on the reservoir proximate to the wellbore (skin), the wider reservoir permeability, reservoir boundaries and many more.

Perhaps even more useful is the provision of information on the overall shape of the network of flow pathways in the reservoir. It has typically been assumed in standard models that this shape is a flat round disc, represented by a radial model grid. The flow pathways converge on the well equally from all horizontal directions, and hence the flow is two-dimensional (2D). For example, this would be the case where permeability is contained within a relatively horizontal formation, and the open-hole section of the well extends through the entire thickness of that formation (full penetration). Flow can also be one-dimensional (1D), with a planar shape. An example of this is where the flow to the well is dominated by flow along a permeable fault. Flow can also be three-dimensional (3D) with a spherical shape, converging on the well equally from all directions including vertically. For example, if the well is located in a formation in which permeability extends above and below the open-hole section (partial penetration). The network of flow pathways can also have some intermediate shape between these 1- 2- and 3- dimensional examples, and the dimension is no longer an integer (fractional dimension).

Knowing the shape is clearly significant to the conceptual model of the geothermal field. Numerical PTA can assess the overall shape of the flow pathways to the well during a test, as different shapes will have characteristic features on the sensitive pressure derivative plot. The block volumes and connection areas of the standard radial grid can be modified to represent different shapes, either by implementing a calculation to alter the dimension of the grid (fractional dimension) or by a calculation to represent reservoir boundaries. The behaviour of the fractional dimension and boundary models are shown in the pressure derivative plot, and then demonstrated with field examples from New Zealand and Iceland.

1. INTRODUCTION

Pressure transient analysis (PTA) involves the analysis of pressure change in a wellbore resulting from changes in flow rate either into or out of the well. It is a highly useful tool that can "see" beyond the wellbore into the reservoir, and is potentially able to assess the condition of the reservoir proximate to the wellbore (damaged or stimulated), and beyond this the characteristics of the wider reservoir, including permeability and shape. Geothermal PTA is often carried out using tools or software based on analytical models, which are relatively simple and cannot adequately represent the high temperatures in the geothermal environment, which is often strongly non-isothermal. In recent years, there has been a push towards using numerical simulators for geothermal PTA, as numerical stimulation is a powerful and flexible tool capable of representing the complexity of geothermal reservoirs and well test scenarios (McLean and Zarrouk, 2017). This movement has led to the development of a framework for numerical PTA (McLean and Zarrouk, 2017), using the simulator TOUGH2 (Pruess, 1991) and controlled by the Python library PyTOUGH (Croucher, 2011). The numerical PTA framework is a guide for reservoir engineers/modellers, with guidelines on the requirements of the grid setup and other simulation parameters. The intention of the numerical PTA framework is to make it easier for reservoir engineers to start using numerical PTA, and to promote comparability of results.

The standard numerical PTA framework has a single-layer radial model grid, which effectively simulates the infinite-acting radial flow (IARF) regime (McLean and Zarrouk, 2017). During IARF the shape of the network of flow pathways is a flat round disc, with flow converging on the well in the horizontal plane, which is two-dimensional (2D) flow. The radial grid can be modified to represent different reservoir shapes, by modification of the block volumes and connection areas. One option is that the reservoir can have boundaries, in which case the grid is 2D radial out to a certain radial distance, beyond which there are impermeable zones in the reservoir, represented by reductions in the block volumes and connection areas. Another option is that the reservoir can have an intrinsic dimension other than 2D, and all the block volumes and connection areas are modified in order to represent a reservoir with a dimension anywhere in the range 1-3. As the dimension need not be an integer, the concept is referred to as fractional dimension (Barker, 1988).

In this study, the fractional dimension numerical PTA model is applied to field data from injection tests into two wells: BR49 at Ohaaki Geothermal Field, New Zealand, and ÞG16 at Þeistareykir Geothermal Field, Iceland. Datasets from both the wells show characteristics of a fractional dimension much less than 2, closer to 1, which is of importance to the conceptual model of the field in each case. It is of additional interest that the ÞG16 dataset exhibits a bend in the falloff, characteristic of a sharp reduction in permeability, as when a fracture, which was stimulated during injection, closes (or partially closes) as the injection flow rate drops. Variable permeability is also implemented into the numerical model as a number of discrete steps.

2. NUMERICAL PTA MODELLING

2.1 Numerical PTA Framework

McLean and Zarrouk (2017) developed the numerical PTA framework due to a dearth of numerical tools/software for geothermal PTA. It provides guidelines on how to set up the model grid and run the simulations, and while it is based on TOUGH2 and PyTOUGH, the guidelines will remain applicable when using other simulators. The numerical PTA framework is based on a single-layer radial model grid, and so the shape of the network of flow pathways is a flat round disc (Figure 1).

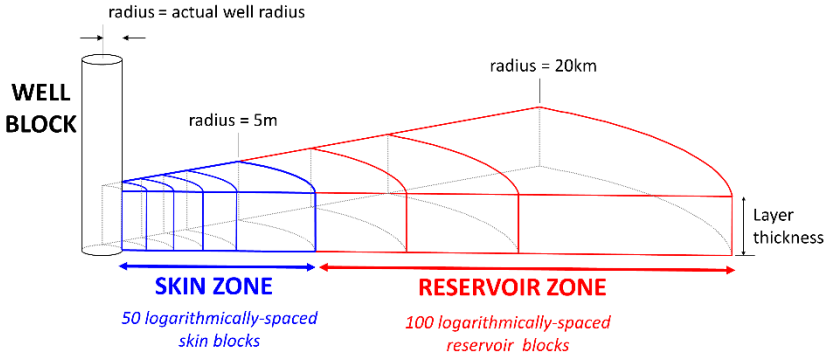

Figure 1: Schematic of single-layer radial model grid from the numerical PTA framework. Only one sector of the full circle is shown, and each block is actually ring-shaped. Not to scale and not all blocks are depicted (modified from McLean and Zarrouk, 2017).

2.2 Fractional Dimension

2.2.1 Concept and Calculations

The block volumes and connection areas of the standard numerical PTA framework grid, which has a dimension of 2.0 (Figure 1), can be modified to represent any dimension n in the range n = 1.0 – 3.0 (from linear to spherical flow) (O'Sullivan et al., 2005). When n = 1.0 there is linear flow, when fluid approaches the well as if along a linear plane (Figure 2) and there is no convergence of flow pathways. If n = 2.0 there is radial flow and fluid converges on the well, moving in the horizontal plane only (Figure 2). When n = 3.0 there is spherical flow, when fluid converges on the well as if from any point on the surface of a sphere, moving towards its centre (Figure 2), and hence there is both horizontal and vertical convergence.

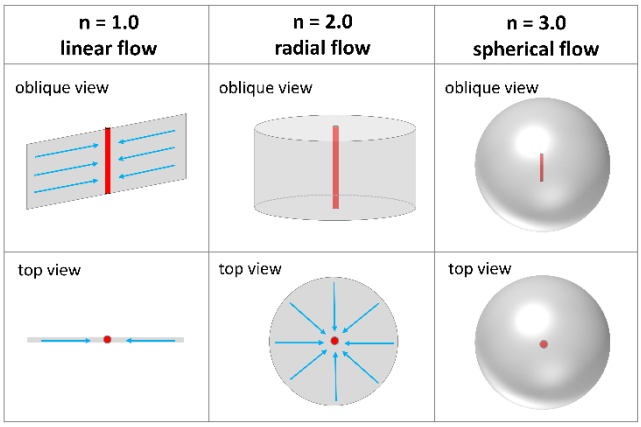

Figure 2: Schematics representing the overall shape of the networks of flow pathways (grey), for values of fractional dimension n=1, 2 and 3. The small red cylinder represents the open-hole section of the wellbore and blue lines representing flow pathways are indicated where practical (not possible for spherical flow).

The block volumes and connection areas on the numerical radial model can be modified using Equation 1 (Barker, 1988), and the equations within Table 1 (O'Sullivan et al., 2005).

$$\alpha_n = \frac{2\pi^{n/2}}{\Gamma(n/2)} \qquad (1)$$

Table 1: Equations to use in combination with the alpha function (Equation 1) to alter a radial model grid to any fractional dimension n in the range 1-3 (O'Sullivan et al., 2005).

Dimension	Volume of i^{th} block (V_i)	Connection area to next-largest block ($A_{i+1/2}$)
1	$2b^2(r_{i+1/2} - r_{i-1/2})$	$2b^2$
2	$\pi b(r^2_{i+1/2} - r^2_{i-1/2})$	$2\pi b r_{i+1/2}$
3	$(4\pi/3)(r^3_{i+1/2} - r^3_{i-1/2})$	$4\pi r^2_{i+1/2}$
n	$(\alpha_n b^{3-n}/n)(r^n_{i+1/2} - r^n_{i-1/2})$	$\alpha_n b^{3-n} r^n_{i+1/2}$

Where: n = fractional dimension in the range 1.0-3.0 (dimensionless); b = "layer" thickness (m) (not the same as the thickness of the original 2D grid shown in Figure 1); r = radial distance from the centre of the well (m).

It should be noted that while the parameter b is the "layer" thickness, it does not have the same meaning as the original layer thickness h of the 2D radial grid as the dimension is not necessarily the same. For the purposes of geothermal PTA, in a fractional dimension grid the well block will always be the same, and then from there outwards the increase in block volumes and surface areas will be controlled by the dimension n. A simple and convenient method is for the first connection area (the well-reservoir interface) to be fixed (Doughty, 2017), which is achieved by calculating the value for b which will make that first connection area in the fractional dimension grid equal to the original first connection area in the 2D radial grid (b will be a function of n). The remaining volumes and connection areas are then calculated from that value of b, and the value of n.

2.2.2 Derivative Plot Model Behaviour

The pressure derivative plot is a highly sensitive and useful plot for PTA, revealing the characteristic shapes of many flow regimes, reservoir and boundary types (McLean and Zarrouk, 2017). The characteristic shape of the fractional dimension model is that in intermediate-time (the reservoir response beyond wellbore storage and the transition hump) the pressure derivative is a straight line. The pressure derivative plot is shown for the range n=1.0-2.0 in Figure 3 and n=2.0-2.6 in Figure 4. When n=2.0 (linear flow) the straight line is flat, which is recognisable as the characteristic IARF response (Figure 3 and Figure 4). When n=1.0 (linear flow) the straight line has a slope of approximately 0.5-log-cycle, and there is a continuum in-between (Figure 3). Theoretically when n=3.0 (spherical flow) the straight line has a slope of approximately negative 0.5-log-cycle, with a continuum in-between, though in practice as n increases the transition hump becomes so large that the straight line reservoir response becomes obscured. The increasing size of the hump (Figure 4) is due to the geometrical skin effect, which has the appearance of positive skin as flow pathways converge on the well from so many directions (Zarrouk and McLean, 2019). The opposite is observed as n decreases (Figure 3) in which case the geometrical skin has the appearance of negative skin (stimulation).

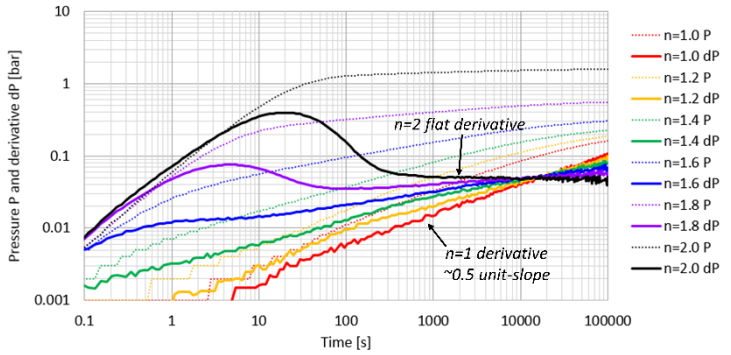

Figure 3: Log-log pressure derivative plot showing characteristic pressure derivative shape for fractional dimension *n* in the range *n* = 1.0 – 2.0.

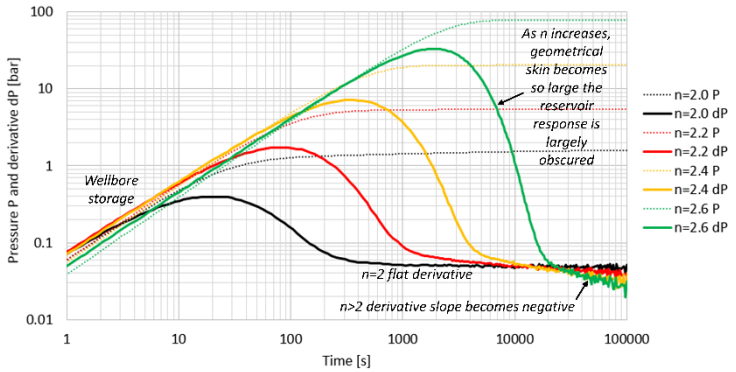

Figure 4: Log-log pressure derivative plot showing characteristic pressure derivative shape for fractional dimension *n* in the range *n* = 2.0 – 2.6.

2.3 Linear Impermeable Boundary

2.3.1 Concept and Calculations

The block volumes and connection areas of the numerical PTA framework radial grid can also be modified using basic geometry equations, to represent linear impermeable boundaries (McLean and Zarrouk, 2015) and in theory boundaries of any shape. This effectively decreases the volumes and areas beyond a certain radial distance, as if part (or all) of the block is no longer there.

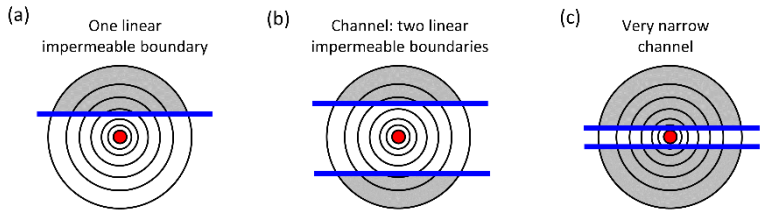

Figure 5: Schematic of radial grids modified with linear impermeable boundaries: (a) one linear impermeable boundary; (b) channel – two linear impermeable boundaries; (c) very narrow channel. Well block = red, boundaries = blue lines, and the part of the model grid "removed" during the calculations = grey shading.

The modified volumes are calculated using the volume of the curved segment (V_{seg}) enclosed between the boundary line and the curve of the block beyond the boundary line (Equation 2) (McLean and Zarrouk, 2015).

$$V_{seg} = h\left(\frac{2\cos^{-1}\left(\frac{L}{r}\right)}{2\pi}\pi r^2 - L\,r\,\sin\left(\frac{2\cos^{-1}\left(\frac{L}{r}\right)}{2}\right)\right) \quad (2)$$

Where: r = block radius (m); L = distance to boundary (m); h = model grid layer thickness (m).

The modified block volume (V_{mod}) is calculated from the original block volume V_0 = original block volume (m^3) and the parameters r, L and h (which give V_{seg}) as follows: if the block radius $r_i \leq L$ then the block is unaffected by the boundary and $V_{modi} = V_{0i}$. For the first block with $r_i > L$, $V_{modi} = V_{0i} - V_{segi}$. For all subsequent blocks with $r_i > L$, $V_{modi} = V_{0i} - V_{segi} + V_{seg(i-1)}$.

The original connection areas (A_0) are simply given by the circumference of the circle times the thickness $A_0 = 2\pi rh$. When block radius $r_i \leq L$ then the block is unaffected by the boundary and the modified connection areas A_{mod} are given by $A_{modi} = A_{0i}$. For all blocks with $r_i > L$, A_{mod} is given by Equation 3, which uses the parameters r, L and h (McLean and Zarrouk, 2015).

$$A_{mod} = 2\,\pi\,r\,h\left(1 - \frac{2\cos^{-1}\left(\frac{L}{r}\right)}{2\pi}\right) \quad (3)$$

2.3.2 Derivative Plot Model Behaviour

The sensitive pressure derivative plot reveals the characteristic shape of the pressure derivative for a single linear impermeable boundary (Figure 6) and two linear impermeable boundaries forming a channel (Figure 7). The model response when the channel is very narrow is similar to the model response for a fractional dimension model of n=1.0 (Figure 3). In both cases, there is negligible transition hump; the well appears stimulated, transitioning directly from the wellbore storage response in early time (unit-slope pressure and derivative) to a linear flow response with ~0.5-unit-slope pressure and derivative, separated but parallel.

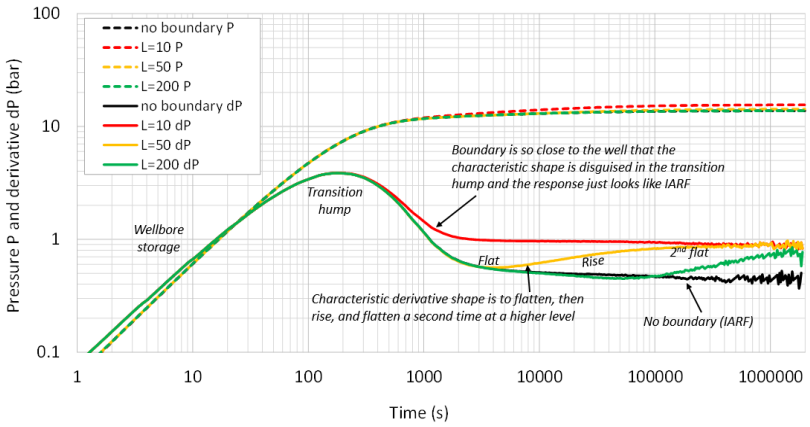

Figure 6: Log-log pressure derivative plot showing characteristic pressure derivative shapes for a single linear impermeable boundary with a well-boundary distance L in the range L = 10-200m, and also the response with no boundary.

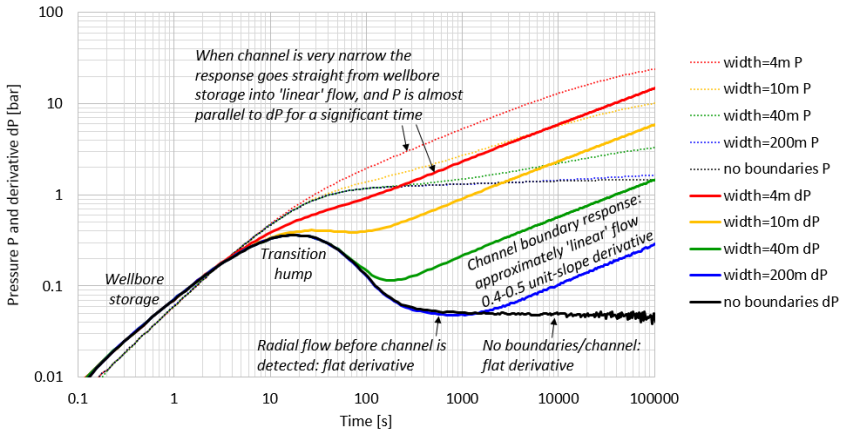

Figure 7: Log-log pressure derivative plot showing characteristic pressure derivative shapes for a channel boundary with a channel width ($2L$) in the range 4-200m and also the response with no boundary.

3. OHAAKI, NEW ZEALAND, WELL BR49

BR49 is a production well in the East Bank of Ohaaki Geothermal Field, New Zealand, drilled in 1995 (McLean et al., 2018). Deflagration was carried out in BR49 in an attempt to increase production from the well. During the deflagration program BR49 was quenched, and full pre-deflagration (test#1) and post-deflagration (test#2) injection tests were carried out, including high-quality long pressure transients. The injectivity of BR49 was 9 t/h/bar pre-deflagration and 13 t/h/bar post-deflagration.

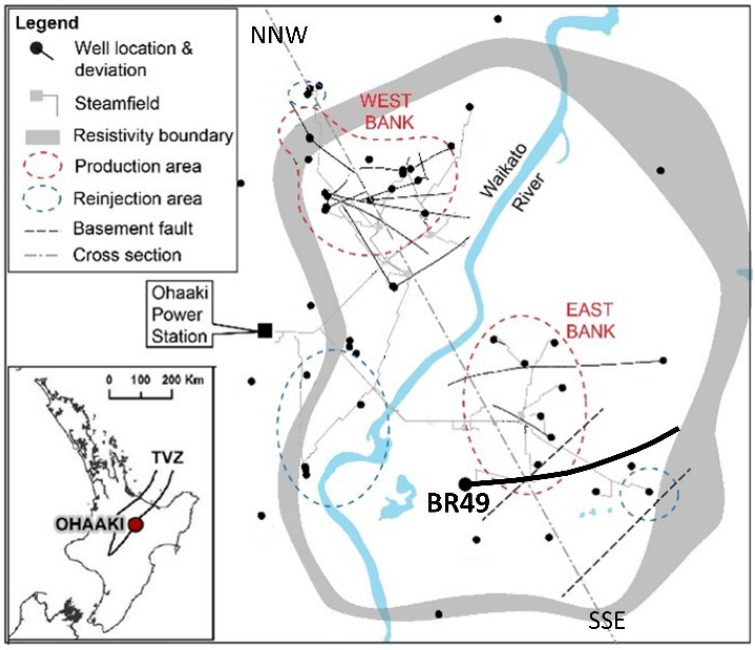

Figure 8: Plan map of Ohaaki Geothermal System showing the West Bank and East Bank production areas, and BR49. The NNW-SSE cross-section line corresponds to Figure 12. Inset: regional map showing the location of Ohaaki geothermal field in the centre of north island of New Zealand (modified from McLean et al., 2018).

3.1 BR49 Field Datasets and Numerical PTA Model Matching

Each injection test has one long transient, a falloff between two injection rates (Figure 9a, Figure 10a). Pressure derivative plots of these falloffs (Figure 9b, Figure 10b) are very similar and exhibit a shape characteristic of almost linear flow, with a straight-line pressure derivative of ~0.5-unit-slope (offset from and parallel to the pressure line). This can be represented by either a fractional dimension model with a low value of n≈1.0 (Figure 3) or a very narrow channel model (Figure 7).

As a side note, both the pressure transient datasets are affected by a regional pressure rebound, as all the wells in the vicinity of BR49 were also shut-in at this time due to a local flash plant outage. This is the cause of the rebound in the pressure ~2 hours into what is supposed to be a falloff, which in the derivative plot causes the pressure data to 'droop' in late-time and the derivative to drop below zero much earlier (Figure 9b, Figure 10b). Despite this interference from the regional pressure rebound, there is still an extensive period (nearly two log cycles) of characteristic almost-linear flow in the derivative plots, permitting model matching. No attempt has been made to include the pressure rebound in the modelling (it was not logged and would be an unconstrained parameter), and in any case this is superfluous to the objective of the modelling in this case. This dataset can be used to determine the shape of the reservoir near the wellbore, using the earlier data. It is interesting as another side note that the model response

exhibits some rebound anyway, even though the regional pressure rebound was not included in the model. The rebound in the model (Figure 9, Figure 10) is the inevitable result of this particular injection test design (superposition of flow steps) with a fractional dimension $n < 2$ (when $n < 2$ the pressure never stabilises between flow steps).

The match between the field data and the fractional dimension model is shown in a derivative plot for the pre-deflagration injection test (Figure 9b) and post-deflagration injection test (Figure 10b). The pre-deflagration falloff has previously been matched with a very narrow channel model by McLean et al. (2018), and the match is shown in Figure 11. A comparison of the estimated parameters n, k (and kh), s, L and P_i from all the modelling is given in Table 2.

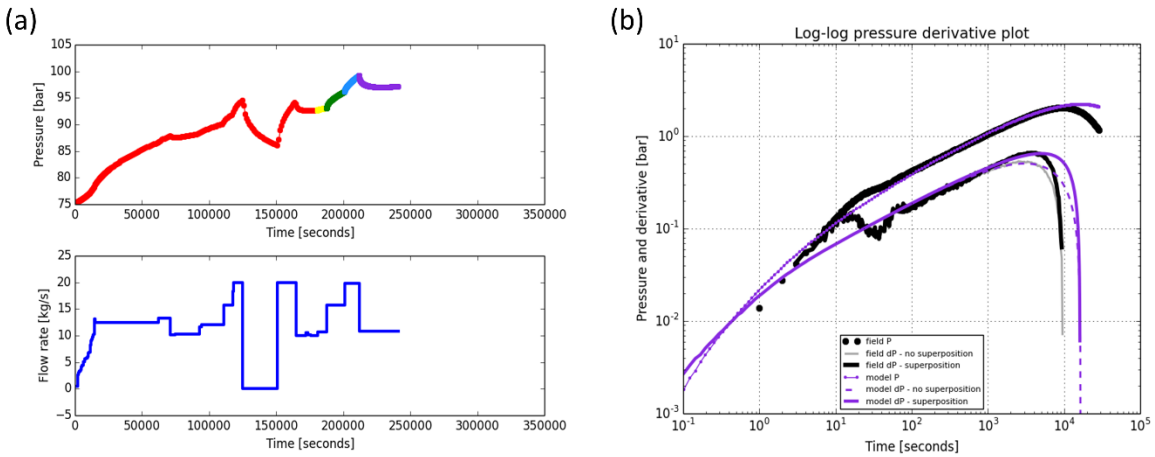

Figure 9: BR49 pre-deflagration injection test 1: (a) history plots of injection flow rate and simulated downhole pressure (the last three steps are the programmed injection test, all prior flow history is quenching or other operational injection. The last step is a drop in injection rate which results in a drop in pressure (purple falloff); (b) field data and fractional dimension model match for the pressure falloff (last step).

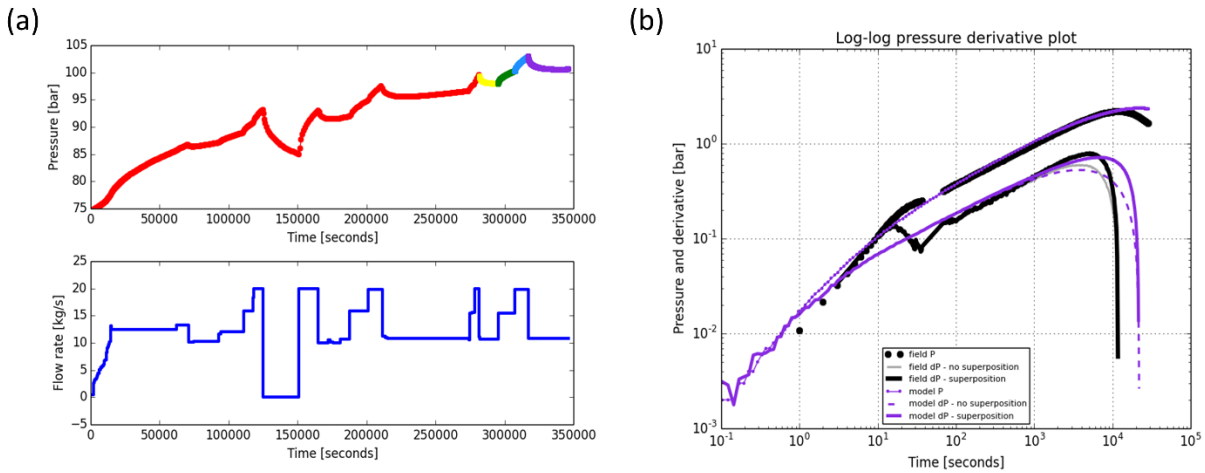

Figure 10: BR49 post-deflagration injection test 2: (a) history plots of injection flow rate and simulated downhole pressure (the last three steps are the programmed injection test, all prior flow history is quenching, other operational injection, and the pre-deflagration injection test. The last step is a drop in injection rate which results in a drop in pressure (purple falloff); (b) field data and fractional dimension model match for the pressure falloff (last step).

Table 2: Comparison of estimated parameters from numerical PTA of BR49 injection tests with the fractional dimension model and very narrow channel model.

		Estimated parameters					
		n	***k***	***kh***	***s***	***L***	***P_i***
Model	**Dataset**	**-**	***e-15 m² (≈mD)***	***e-12 m³ (≈D.m)***	**-**	***m***	***bara***
Fractional Dimension	Falloff #1 (pre-deflag)	1.05	4400	4752	-2	-	75.36
	Falloff #2 (post-deflag)	1.05	4700	5076	-2	-	74.75
Very Narrow Channel	Falloff #1 (pre-deflag)	-	66	71	0.2	2.5	77.0

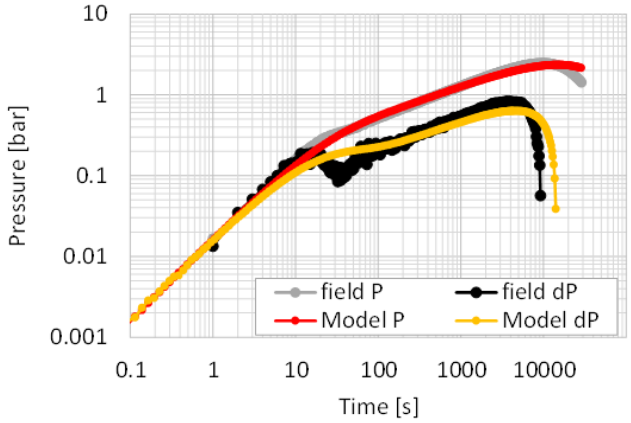

Figure 11: BR49 pre-deflagration injection test 1: derivative plot of field data and very narrow channel model match for the pressure falloff (McLean et al., 2018).

3.2 Significance of BR49 Results for Conceptual Model

In the case of BR49 the results of PTA are highly significant for the conceptual model of Ohaaki Geothermal Field (McLean et al., 2018). Over the years there has been debate over whether there is one upflow at Ohaaki (in the West Bank), or two upflows (one in the West Bank and another one in the East Bank). The two-upflow conceptual model is shown in cross-section in Figure 12.

The BR49 falloffs can be matched with either a fractional dimension model with a very low value of *n* (close to 1), or a very narrow channel model, both indicating that the flow to BR49 is very much confined, as along an almost linear planar feature. The only such feature likely to exist in the vicinity of BR49 is a fault, as the major feed zone in BR49 is located in the usually-impermeable greywacke basement, within which permeability is only secondary, along faults/fractures (McLean et al., 2018).

Therefore, it was concluded that BR49 has been drilled into an upflow along a basement fault, under the East Bank. This result from numerical PTA provides important confirmation for the two-upflow conceptual model (Figure 12). This two-upflow conceptual model is also supported by other data sources including geophysics (magnetotelluric data), numerical modelling of the whole field, geology, and long-term trends in the reservoir geochemistry and reservoir pressure (McLean et al., 2018). The results of numerical PTA are available much earlier than most of these other data sources, and are therefore of extreme importance to the conceptual model.

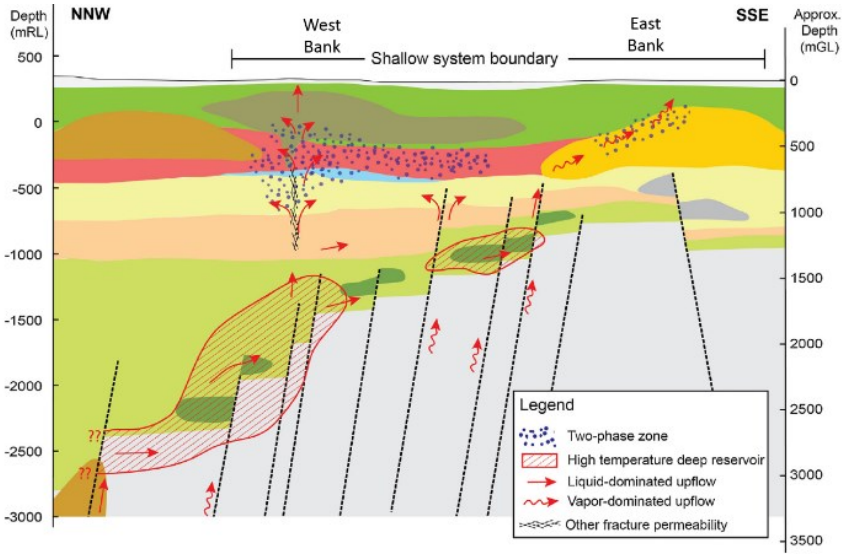

Figure 12: Two-upflow conceptual model at Ohaaki Geothermal Field (McLean et al., 2018, after Mroczek et al., 2016).

4. ÞEISTAREYKIR, ICELAND, WELL THG16

ÞG16 is a production well for the Þeistareykir power plant, drilled in 2017 to intersect expected fracture permeability under the nearby Mt Bæjarfjall in the south of the field (Figure 13) (Guðjónsdóttir et al., 2017). Injection testing was carried out at well completion, during which three pressure transients were captured: two buildups between injection rates, and one falloff between injection rates. The injectivity of ÞG16 is 8 t/h/bar (converted from 2.2 L/s/bar).

4.1 ÞG16 Field Datasets and Numerical PTA Model Matching

The injection/completion test on ÞG16 had three step changes in flow rate following an extended period of injection during drilling and other downhole activities (Figure 14). The injection prior to the injection/completion test was estimated from circulation losses

during drilling and other injection records prior to the completion test. It is necessary to include an estimate of this early injection, not because superposition from those steps will have any significant impact on the field pressure derivative, but because it will have a significant impact on the model response. Without inclusion of the early injection, the model starts injecting cold water into a hot reservoir that has not been cooled at all during drilling, and so non-isothermal effects will dominate and distort the modelled response and the characteristic derivative shapes (e.g. Figure 3, Figure 4) will not be seen.

High-quality data has been captured for the two buildups and the falloff (between flow rates), permitting a comparison between results from different steps. The ÞG16 falloff (Figure 14, in purple) exhibits an interesting feature: there is a bend in the falloff around 5000 seconds (just over 1.5 hours). This feature is often referred to as a "fracture closing" (Bakar and Zarrouk, 2018; Zarrouk and McLean, 2019) which can occur in wells that are stimulated during injection, but experience a sudden sharp decline in permeability as pressure drops during falloff. This is more likely to occur in relatively impermeable wells which show signs of stimulation during injection, which is consistent with the low injectivity of ÞG16 and the increase in permeability required for the model matching of the buildups.

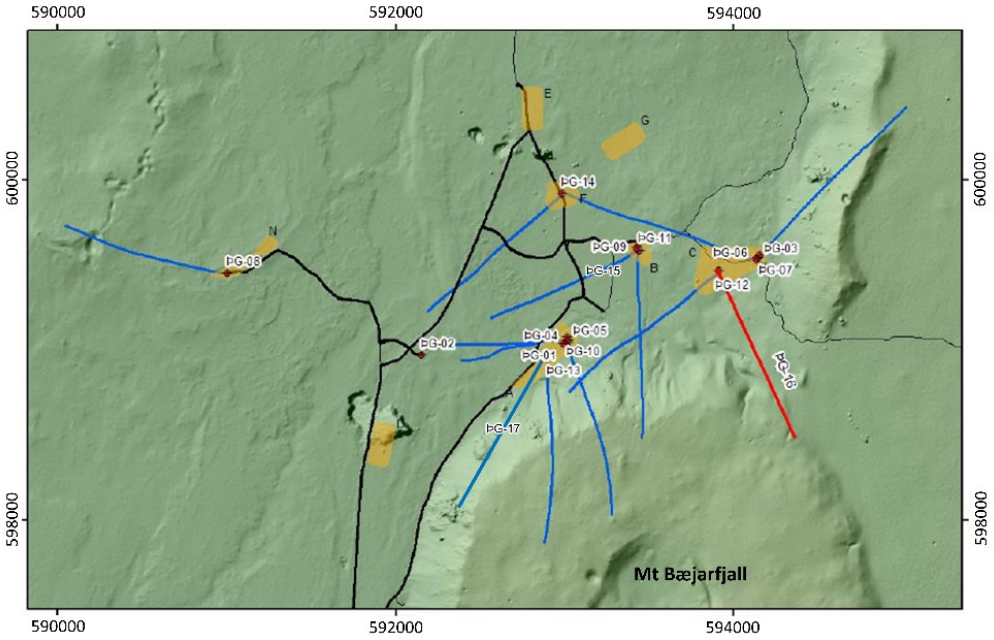

Figure 13: Map of Þeistareykir Geothermal Field with topography, well tracks, and ÞG16 in red. Mt Bæjarfjall is located in the south (modified from Guðjónsdóttir et al., 2017).

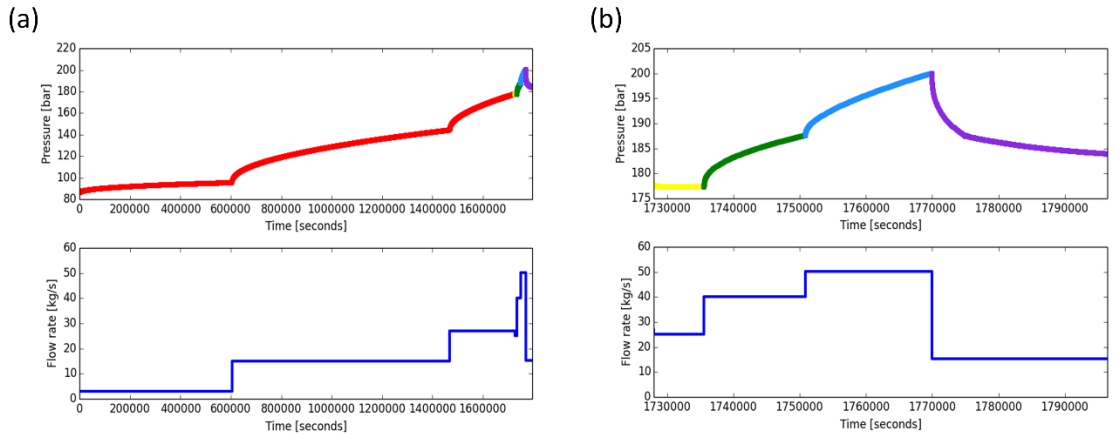

Figure 14: ÞG16 completion/injection test, illustrated with plots of flow rate and simulated pressure: (a) for the injection test and all prior injection; (b) zoom in on the injection test only.

For Step 1, Step 2 and Step 3 (green, blue and purple in Figure 14), the field data and model match (fractional dimension model with changing permeability) are shown in history and pressure derivative plots in Figure 15, Figure 16 and Figure 17, respectively. The estimated parameters are summarised in Table 3.

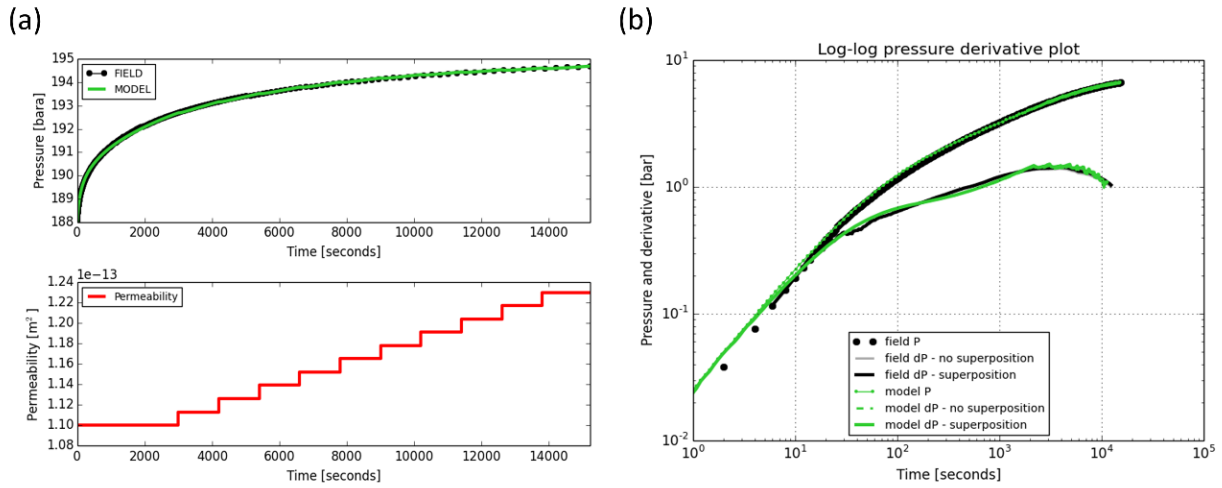

Figure 15: ÞG16 injection test Step 1 (buildup) field data and match with fractional dimension/changing permeability model: (a) History plots of pressure and permeability; (b) Pressure derivative plot.

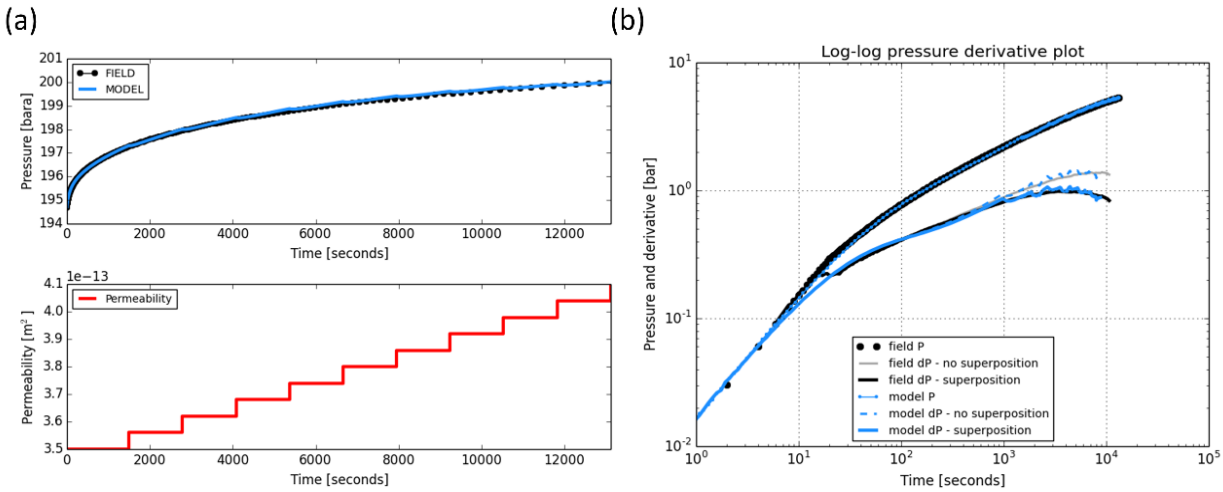

Figure 16: ÞG16 injection test Step 2 (buildup) field data and match with fractional dimension/changing permeability model: (a) History plots of pressure and permeability; (b) Pressure derivative plot.

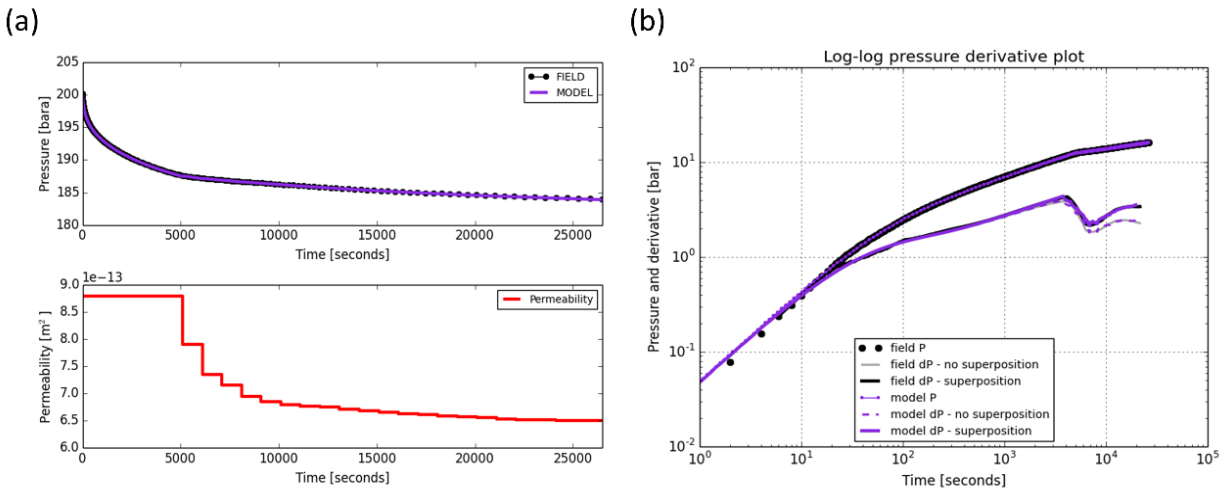

Figure 17: ÞG16 injection test Step 3 (falloff) field data and match with fractional dimension/changing permeability model: (a) History plots of pressure and permeability; (b) Pressure derivative plot showing match between model and field data.

Table 3: Comparison of estimated parameters from numerical PTA of ÞG16 injection test Steps 1, 2 and 3 (Figure 15, Figure 16, Figure 17) with the fractional dimension/changing permeability model.

	Estimated parameters				
	n	***k1 – k2***	***kh1 – kh2***	***s***	***P_i***
Dataset	**-**	***e-15 m^2 (≈mD)***	***e-12 m^3 (≈D.m)***	**-**	***bara***
Step 1: buildup	1.3	110 - 123	166 - 186	-3.8	135.6
Step 2: buildup	1.2	350 - 410	529 - 619	-3.8	125.0
Step 3: falloff	1.1	880 - 650	1329 - 982	-3.8	86.3

The fractional dimension of the reservoir is likely to be in the range 1.1 – 1.3 (Table 3), and more likely to be closer to 1.1 as this is the result for Step 3 which has the highest data quality. The value of skin factor was not kept constant when modelling each step, it was a variable parameter. As the estimated value turned out to be the same for each step, it has a high level of confidence. The value of s=-3.8 indicates a high level of stimulation of the near-wellbore reservoir during the injection test. This is consistent with the stimulation/increasing permeability modelled for Steps 1 and 2.

4.2 Significance of ÞG16 Results for Conceptual Model

ÞG16 is located in the southeast of Þeistareykir Geothermal Field, and northeast of Mt Bæjarfjall (Figure 13). The current conceptual model in that area is that ÞG16 is likely producing from a different compartment to the other wells, as the geochemical signature is quite different (in terms of oxygen isotopes), and the enthalpy is lower than expected. There are some large tectonic structures in the field that could be an impermeable barrier between ÞG16 and the other wells. Interestingly, the water appears to have not reacted much with the rock although it dates back to the ice age.

The ÞG16 numerical PTA clearly indicates that this is an unusual well, with a low value of fractional dimension n = 1.1-1.3. This is unusually low, as production wells in highly fractured volcanics would be expected to have a value of n close to 2, or even greater than 2 as fracture networks branch out from the well. This is indeed the case for three other production wells analysed in the main productive part of the reservoir (indicated in light blue in Figure 19), which all have a fractional dimension in the range n=2.0-2.2. The range of values n = 1.1-1.3 indicates that shape of the network of flow pathways around this well is not quite linear (it must branch out somewhat), but is still very much confined, with much less convergence of flow pathways than for 'normal' radial flow. The target of ÞG16 was fracture permeability anticipated to be located under Mt Bæjarfjall. The implication of the low value for fractional dimension is that the fracture permeability found in that location is quite confined and not well-connected to the wider fracture network in the main productive part of the reservoir. This supports the current conceptual model with ÞG16 producing from a different compartment, and provides a reason for the reservoir compartmentalisation.

Further information regarding the fracture network around ÞG16 is available from acoustic wellbore imaging, which covers the entire open-hole section of the well (Þorsteinsdóttir et al., 2018). The orientation of the fractures identified from the image with a high level of confidence (214 fractures) are oriented in the range N-S to NNE-SSW, dipping steeply to the WNW (Figure 18, Þorsteinsdóttir et al., 2018). This includes the "open fractures" most likely to be pathways for fluid flow, which are those visible or partially visible in the acoustic travel time image. When the orientation of the fracture network around ÞG16 is considered relative to the other wells, the reason for the "compartmentalisation" - or simply lack of connectivity into the main productive reservoir - is easily apparent (Figure 19): the fracture network does not extend out from the wellbore in the direction of any of the other production wells. The relatively impermeable rocks which are not part of the fracture network lie between ÞG16 and the main productive reservoir, and also lie on the other side of ÞG16, forming the eastern (or southeastern) field boundary (Figure 19).

While the acoustic borehole image alone provides the orientation of the fracture network at ÞG16, the very low fractional dimension (n = 1.1-1.3) provides the additional critical information that the network is greatly confined and does not diverge that much away from the well. It is possible for example for a well to have a dominant fracture orientation, and yet a fractional dimension around 2 (approximately radial flow), as is the case for wells at Wairakei Geothermal Field, New Zealand, which has very different implications for the overall shape of the fracture network and therefore the conceptual model. It is necessary to consider the fractional dimension and the orientation from the borehole image in combination, in order to form a meaningful interpretation relevant to the conceptual model.

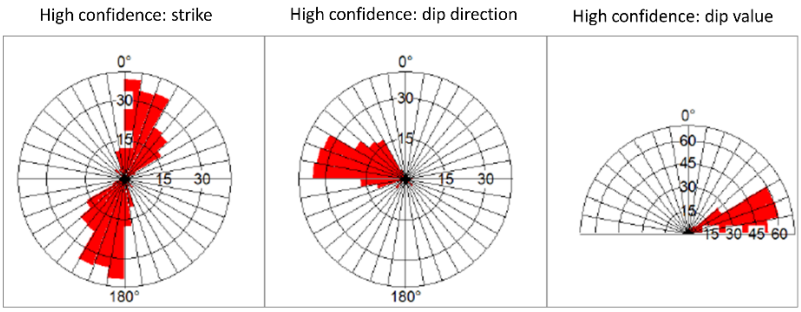

Figure 18: Rose diagrams for high-confidence fractures identified in the acoustic wellbore image from ÞG16 (Þorsteinsdóttir et al., 2018).

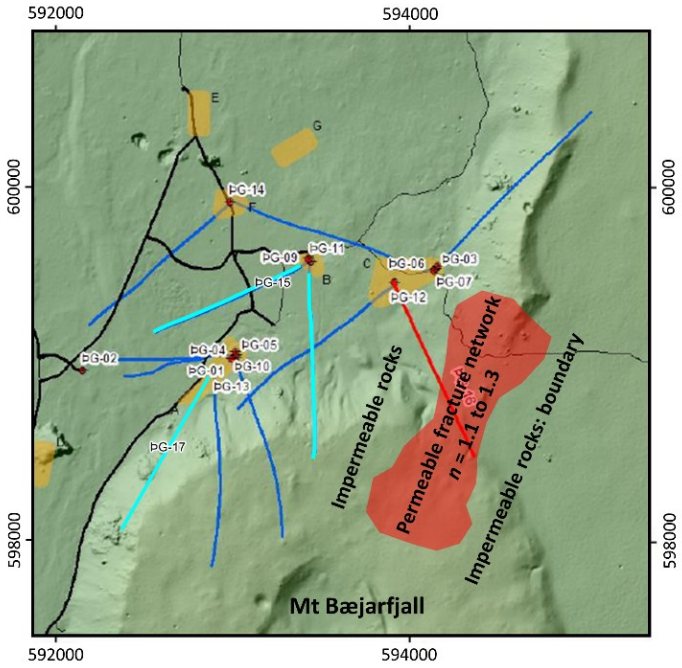

Figure 19: Sketch map of Þeistareykir Geothermal Field showing some key conceptual model features indicated by the numerical PTA and wellbore imaging in the vicinity of ÞG16 (modified from Guðjónsdóttir et al., 2017).

5. OTHER DISCUSSION

5.1 Assessment of future production potential

The value of *kh* is often used as an indicator of the future production potential of a well. For example the threshold for a "good" production well in New Zealand is approximately $kh = 10 \times 10^{-12}$ m^3, though this can vary between fields. When using the fractional dimension model, it is important to note that values of *kh* are not directly comparable for different values of fractional dimension *n*. The threshold of $kh = 10 \times 10^{-12}$ m^3 is valid for $n = 2.0$, where fluid pathways are converging on the well radially from all horizontal directions. Another well can have the same value of *kh* but because the fractional dimension is $n = 1.0$ (Figure 20) the volume of the reservoir is significantly less and the well will not be a good producer. This does not mean that wells with $n = 1.0$ cannot be good producers, BR49 has $n = 1.05$ and is a good production well. It simply means that when *n* is low, the value of *k* must be much higher for the well to be a good producer. Therefore the threshold of $kh = 10 \times 10^{-12}$ m^3 for $n = 2.0$ will have to be much higher when $n = 1.0$ and lower when $n = 3.0$.

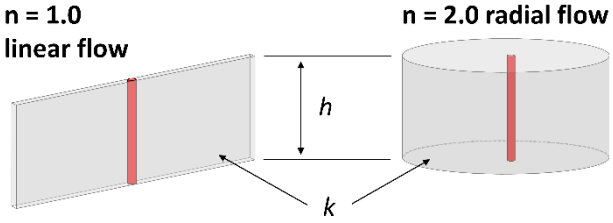

Figure 20: Schematic illustrating two reservoirs with the same value of kh but different fractional dimension n.

And so *kh* becomes some non-linear function of *n*, as illustrated by the BR49 results, which are $kh \approx 5000 \times 10^{-12}$ m^3 for $n = 1.05$. Using the old threshold ($kh = 10 \times 10^{-12}$ m^3), this would indicate an astronomically good well as 5000 >> 10. However this is not consistent with the injectivity of the well, which is 9-13 t/h/bar, which reasonable but not fantastic. The threshold for $n = 1.05$ must in fact be much higher than 10×10^{-12} m^3, but less than 5000×10^{-12} m^3. Establishing the threshold for a 'good' well as a function of *n* is more of a long-term project (for the future), requiring PTA results from multiple wells, and other indicators of well performance such as injectivity or productivity. For now, it is sufficient to remember not to get too excited about a high value of *kh* if $n < 2$, and conversely not to be too disappointed about a low value of *kh* if $n > 2$.

This also explains why the BR49 results for *kh* are so different between the fractional dimension models and the channel model (Table 2). The fractional dimension model has the much higher value of $kh \approx 5000 \times 10^{-12}$ m^3 and as it is nearly linear ($n = 1.05$), the reservoir is very narrow, only the width of the wellbore near the well (~0.2 m), and expanding only slightly with distance from the well. The channel model has the lower value of $kh = 71 \times 10^{-12}$ m^3, which makes sense as the reservoir is quite a lot wider in this case (5 m). It is apparent that values of *kh* should be interpreted with caution.

6. CONCLUSIONS

The primary conclusions of this study are as follows:

- The implementation of fractional dimension and changing permeability into the numerical PTA framework has proven effective for modelling multiple pressure transient datasets (buildups and falloffs) from the wells BR49 at Ohaaki, New Zealand and ÞG16 at Þeistareykir, Iceland.
- The numerical PTA results from BR49 are of significant importance to the conceptual model of the Ohaaki Geothermal Field, clearly supporting the two-upflow model. The results from either the fractional dimension model or the very narrow channel model point towards this same conclusion.
- The numerical PTA results from ÞG16 are of significant importance to the conceptual model of the Þeistareykir Geothermal Field, providing an explanation for the apparent compartmentalisation in the vicinity of ÞG16.
- The fractional dimension from PTA and fracture orientation data from wellbore imaging provide a powerful combination to make meaningful interpretations for conceptual models.
- The changing permeability model has proved effective for two purposes: modelling the common phenomenon of stimulation/increasing permeability during geothermal buildups and modelling the less-common phenomenon of sudden decline in permeability during falloffs (due to fracture closing) in relatively impermeable geothermal wells.
- The threshold *kh* value for a "good" well is dependent on the fractional dimension *n*. The threshold becomes significantly and non-linearly higher as *n* decreases below 2, and conversely, the threshold is non-linearly lower as *n* increases above 2.

ACKNOWLEDGEMENTS

The authors gratefully acknowledge the following organisations: the Todd Foundation for financial support, Contact Energy for financial support and access to data, and Landsvirkjun for access to data.

REFERENCES

Bakar, H. A. and Zarrouk, S. J.: Transient pressure analysis of geothermal wells fractured during well testing, *Geothermics*, **76**, (2018), 26-37.

Barker, J. A.: A generalized radial-flow model for pumping tests in fractured rock, *Water Resources Research*, **24**(10), (1988), 1796-1804.

Croucher, A. E.: PyTOUGH: a Python Scripting Library for Automating TOUGH2 Simulations, *Proceedings*, 33rd New Zealand Geothermal Workshop (2011).

Doughty, C.: Generating one-column grids with fractal flow dimension, *Computers and Geosciences*, **108**, (2017), 33-41.

Guðjónsdóttir, S.R., Sigurgeirsson, M. Á., Ásgeirsdóttir, R. S., Guðmundsdóttir, V., Tryggvason, H. H., Egilson, Þ., Pétursson, F., Gunnarsson, B. S., Ingólfsson, H. and Vilhjálmsson, S.: Þeistareykir – Well ÞG-16. Phase 3: Drilling for a 7" Perforated Liner down to 2702 m, ISOR *client report* 2017/046 to Landsvirkjun, August (2017).

McLean, K., McDowell, J. M., Sepulveda, F., Seastres, J., Zarrouk, S. J. and Alcaraz, S.: Upflow along a basement fault revealed by geothermal numerical pressure transient analysis, *Proceedings*, 40th New Zealand Geothermal Workshop, Taupo, New Zealand, 14-16 November (2018).

McLean, K. and Zarrouk, S. J.: Pressure transient analysis of geothermal wells: a framework for numerical modelling, *Renewable Energy*, **101**, (2017), 737-746.

McLean, K. and Zarrouk, S. J.: Linear impermeable boundary in geothermal pressure transient analysis: a reservoir modelling assessment, *Proceedings*, 37th New Zealand Geothermal Workshop, Taupo, New Zealand, 18-20 November, (2015).

Mroczek, E., Milicich, S., Bixley, P., Sepulveda, F., Bertrand, E., Soengkono, S. and Rae, A.: Ohaaki geothermal system: refinement of a conceptual reservoir model, *Geothermics*, **59**, (2016), 311-324.

O'Sullivan, M. J., Croucher, A. E., Anderson, E. B., Kikuchi, T. and Nakagome, O.: An automated well-test analysis system (AWTAS), *Geothermics*, **34**(1), (2005), 3-25.

Pruess, K.: TOUGH2: A general-purpose numerical simulator for multiphase fluid and heat flow, Lawrence Berkeley Report No. LBL-29400, Berkeley, California (1991).

Þorsteinsdóttir, U., Árnadóttir, S., Gautason, B., Gunnarsson, B.S., Pétursson, F., Ingimarsson, H. and Þorsteinn Egilson, Þ.: Well ÞG-16: Results of Televiewer Imaging at the Þeistareykir Geothermal Field, NE-Iceland, ISOR *client report* 2018/101 to Landsvirkjun, December (2018).

Zarrouk, S. J. and McLean, K.: Geothermal Well Test Analysis: Fundamentals, Applications and Advanced Techniques, 1st edition, (2019), Elsevier.